

Walk dimension for light in complex disordered media

Romolo Savo^{1,2,*}, Matteo Burrelli^{1,3}, Tomas Svensson¹, Kevin Vynck^{1,4,†} and Diederik S. Wiersma^{1,2,3}

¹*European Laboratory for Non-linear Spectroscopy (LENS), 50019 Sesto Fiorentino (FI), Italy*

²*Università di Firenze, Dipartimento di Fisica e Astronomia, 50019 Sesto Fiorentino (FI), Italy*

³*Istituto Nazionale di Ottica (CNR-INO), Largo Fermi 6, 50125 Firenze (FI), Italy and*

⁴*Institut Langevin, ESPCI ParisTech, CNRS, 1 rue Jussieu, 75238 Paris Cedex 05, France*

Transport in complex systems is characterized by a fractal dimension – the walk dimension – that indicates the diffusive or anomalous nature of the underlying random walk process. Here we report on the experimental retrieval of this key quantity, using light waves propagating in disordered media. The approach is based on measurements of the time-resolved transmission, in particular on how the lifetime scales with sample size. We show that this allows one to retrieve the walk dimension and apply the concept to samples with varying degree of fractal heterogeneity. In addition, the method provides the first experimental demonstration of anomalous light dynamics in a random medium.

I. INTRODUCTION

Despite its conceptual simplicity a random walk can describe several and very different transport phenomena. Examples include heat transport [1], animal foraging [2], human travel [3], molecular diffusion [4], and the propagation of waves in random media [5, 6]. A fundamental aspect of random walks in disordered media is the scaling property of the dynamics, which is commonly expressed by the following type of propagator [7, 8]:

$$W(\mathbf{r}, t|\mathbf{r}') = t^{d_w/d_f} \tilde{W}\left(\frac{|\mathbf{r} - \mathbf{r}'|}{t^{1/d_w}}\right), \quad (1)$$

where \tilde{W} is an invariant profile function, d_f is the (mass) fractal dimension of the system and d_w is the walk dimension (namely the fractal dimension of the random walk). This relation expresses the general fact that the propagator W , which provides the probability density to find a random walker in point \mathbf{r} at time t starting from \mathbf{r}' at $t = 0$, can be rescaled onto \tilde{W} at any time t . Most importantly, the propagator W is expected to spread asymptotically with the characteristic length $\xi(t) \sim t^{1/d_w}$. As the value of the walk dimension reveals unambiguously whether the process is diffusive ($d_w = 2$), subdiffusive ($d_w > 2$) or superdiffusive ($d_w < 2$), it has become a key observable in the anomalous transport research [7, 9, 10]. Measurements have been performed on the random walk of small objects, like particles and molecules [4, 11–16]. In these cases, the actual trajectories of the objects could be monitored in time *inside* the complex medium and thus Eq. (1) could be directly tested. Similarly to massive objects, multiply scattered waves in disordered media may also propagate anomalously [6, 17], in which case

the experimental retrieval of d_w is particularly challenging. In recent years superdiffusion of light has been investigated in disordered photonics materials dubbed Lévy glasses [18, 19] and in hot atomic vapors [20, 21]. However, neither experiments on the dynamics of anomalous transport have been performed nor the walk dimension d_w has been measured.

Here we report on the experimental retrieval of the fractal dimension of an optical random walk, by analyzing the scaling of the time-resolved transmission with sample size. We show that this type of analysis can clearly distinguish between different transport regimes - from diffusive to superdiffusive - consistent with the topology of the system. Apart from the retrieval of d_w for an optical random system, this study also provides a direct confirmation of superdiffusion in Lévy glasses. The concept is general and applies to other transport phenomena.

II. SAMPLES AND EXPERIMENT

Lévy glasses provide a convenient playground for the investigation of anomalous diffusion since their structural parameters can be readily varied. Moreover, the use of light waves has the enormous advantage that transport can be studied via simple observables, and a large statistics can be accumulated. The Lévy glasses used in these experiments are obtained by embedding glass microspheres with diameter ϕ distributed with a power-law, $p(\phi) \sim \phi^{-(\beta+1)}$, into an index-matched polymer matrix containing randomly dispersed TiO₂ nanoparticles (See Appendix A). Light is scattered by the nanoparticles in between the microspheres, while propagating freely inside them. The power-law heterogeneity size distribution $p(\phi)$ is created to yield a heavy-tailed step length distribution for the random walk of light, and is expected to lead to superdiffusion [18, 19]. The “degree of superdiffusivity” may then be controlled via the exponent β at the sample preparation stage. The structure is contained between two glass slides, index-matched with the polymer matrix and the microspheres, with the sample thickness L ap-

* romolo.savo@lkb.ens.fr; Current affiliation: Laboratoire Kastler Brossel, UMR 8552, CNRS, Ecole Normale Supérieure, Université Pierre et Marie Curie, Collège de France, 24 rue Lhomond, 75005 Paris, France

† Current affiliation: Laboratoire Photonique, Numérique et Nanosciences (LP2N), UMR 5298, CNRS - IOGS - Univ. Bordeaux, Institut d’Optique d’Aquitaine, 33400 Talence, France

proximately equal to the largest sphere diameter.

Measurements were also performed on samples containing an homogeneous random distribution of nanoparticles. These were obtained by substituting the microspheres of Lévy glasses with an equivalent volume of polymer. Such samples are expected to be diffusive and differ from Lévy glasses only in the spatial distribution of scatterers. In addition, given the equal volume-averaged density of nanoparticles, it is expected that the step length distribution of these samples differs from Lévy glasses only in its second moment but not in its first moment (i.e., equal mean step) [22].

The experiment was performed by shining 130 fs laser pulses at 810 nm wavelength on the sample and collecting the transmitted light. By adopting a nonlinear optical gating technique [23–25] we monitor the temporal profile of the transmission with sub-ps resolution [Fig. 1(a)] (see Appendix B).

III. RESULTS AND DISCUSSION

A. Time-resolved transmission

Figure 1(b) shows a series of measurements of the time-resolved transmission performed on a Lévy glass ($\beta = 2.0$, $L = 434 \mu\text{m}$) for different injection points on the sample surface. The strong dependence of the early-time profile with the injection point is evident, in sharp contrast with the late-time behavior, where an exponential tail $\exp(-t/\tau)$ with a well-defined lifetime τ is observed (see the inset). The intensity fluctuation at early times is transient, and due to the large-scale heterogeneities of the sample [26, 27] which allow light to escape from deep inside in only a few scattering events. The fluctuations vanish at times larger than τ , which is approximately the time needed to explore all regions of the sample (the Thouless time [28]) and reach ergodicity. This transient, position-dependent, dynamics is not observed in statistically homogeneous systems.

Figure 1(c) shows the comparison between the time-resolved transmission of the Lévy glass and the reference homogeneous sample. The average profile for the homogeneous sample does not exhibit any sharp features at early times, as expected. A fit with diffusion theory [29] returns a transport mean free path $\ell_t = 40 \mu\text{m}$, which we shall take as the mean step length $\langle \ell \rangle$ in our Lévy glasses.

B. Lifetime scaling with sample thickness

As shown in Ref. [30], the time-resolved transmission is expected to verify asymptotically the following scaling behavior:

$$T(t, L) = L^\gamma \tilde{T}\left(\frac{L}{\xi(t)}\right), \quad (2)$$

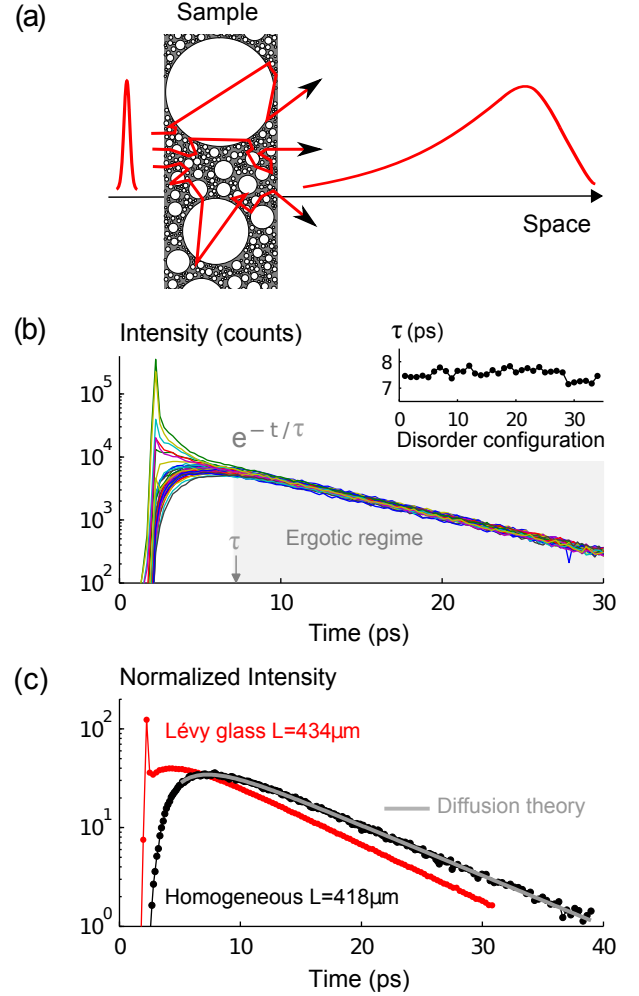


FIG. 1. (Color online) Time-resolved transmission. (a) Sketch of the experimental setting. A sub-ps laser pulse is incident onto a Lévy glass and the time-resolved transmission is measured. (b) Measured time-resolved transmission for a Lévy glass with $\beta = 2.0$ and $L = 434 \mu\text{m}$ for different injection points on the surface. The early-time response strongly depends on the source position while at late times, the intensity decays exponentially with a narrow lifetime distribution (see the inset). (c) Average time-resolved transmission for the Lévy glass in (b) and a homogeneous sample. The two samples have a comparable thickness and the same volume-averaged density of TiO_2 nanoparticles. The curves have been normalized to the laser pulse power. The time-resolved transmission responses are strikingly different, indeed the first light arrives later and the lifetime is longer for the homogeneous sample. A fit with diffusion theory returns a transport mean free path $\ell_t = 40 \mu\text{m}$.

where \tilde{T} is an invariant transmission function and γ a characteristic exponent related to the steady-state transmission properties. Furthermore, given the exponential tail of the transmission curve $T(t) \sim \exp(-t/\tau)$ (see Fig. 1), we expect the lifetime to scale as $\tau \sim L^{d_w}$. Hence, we performed time-resolved transmission experiments on

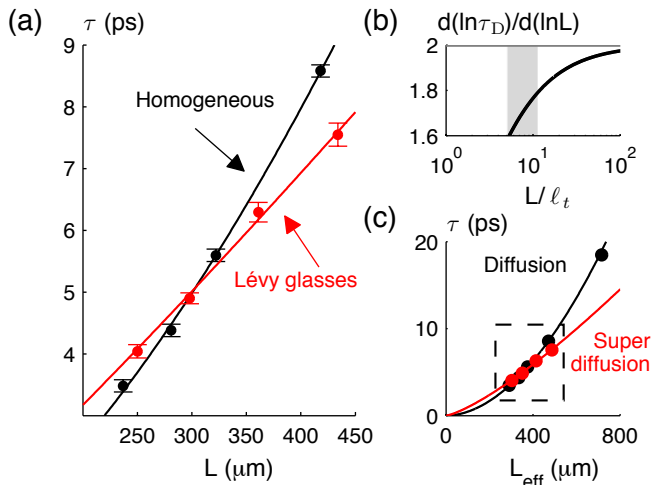


FIG. 2. (Color online) Scaling of lifetimes. (a) Lifetimes versus sample thickness for the $\beta = 2.0$ Lévy glass and the homogeneous media. Error bars give the standard deviations of measurements performed in different injection points. Markedly different scaling trends are found. The scaling exponent z is obtained from the fit $\tau = bL^z$ (continuous lines). (b) Calculation of $d(\ln\tau_D)/d(\ln L)$ versus L from diffusion theory shows the effect of finite system size on the evaluation of z . The highlighted interval corresponds to the thickness range of investigation which returns a value in good agreement with the measured one. (c) The scaling exponent d_w is retrieved from the fit $\tau = cL_{\text{eff}}^{d_w}$. The additional reference data point shows that at larger L the deviation between diffusive and superdiffusive scaling is expected to be even clearer. Unfortunately, so far, we could not realize reliable Lévy glasses at larger thicknesses. The fits for the two data sets are performed on the same thickness range.

samples with different thicknesses to retrieve the scaling exponent d_w . We considered Lévy glasses with two heterogeneity size distributions ($\beta = 2.0$ and 2.6) and the corresponding homogeneous samples. The volume-averaged density of nanoparticles was kept constant in all samples for the sake of comparison. The importance of this point will be discussed later on. The lifetime τ was obtained from the decay at long times, using an average over 30 different injection points, leading to a standard deviation smaller than 3%.

As we are considering real (finite) systems a quantitative analysis of their scaling properties requires to account for the presence of boundaries. However, we prefer to start by showing the raw data since they already allow for important physical considerations. Figure 2(a) shows the measured τ as a function of L for Lévy glasses with $\beta = 2.0$ and the homogeneous samples. Their dependence with sample thickness turns out to be very different, as a consequence of a pure spatial redistribution of the scatterers. We quantify this difference by performing a fit to the data with a generic power-law function $\tau = bL^z$, where b is a constant and z is the measured scaling exponent. The fits return $z = 1.1 \pm 0.2$ for the

Samples set	z	d_w
Lévy Glasses $\beta=2.0$	1.1 ± 0.2	1.3 ± 0.3
Lévy Glasses $\beta=2.6$	1.3 ± 0.2	1.5 ± 0.2
Homogeneous samples	1.6 ± 0.2	1.9 ± 0.2

TABLE I. Measured scaling exponents. The values reported for z and d_w have been obtained as best fit exponents of the functions $\tau = bL^z$ and $\tau = cL_{\text{eff}}^{d_w}$, respectively. Errors have a statistical confidence of 95%.

Lévy glass and $z = 1.6 \pm 0.2$ for the homogeneous media, thereby revealing a remarkably different dynamics. The smaller z in the Lévy glass indicates a faster growth of the characteristic length ξ with time, originating from the heavy-tailed step length distribution. The same analysis performed on the $\beta = 2.6$ Lévy glass yields $z = 1.3 \pm 0.2$. This shows that the light transport dynamics is dictated by the heterogeneity size distribution, via the β exponent.

We now consider the effect of system finiteness on the evaluation of the scaling exponent. It is well known that the diffuse lifetime in finite systems should scale as $\tau_D \propto (L + 2z_e)^2$, where z_e is the so-called “extrapolation length” [5]. Since $z_e = \frac{2}{3}\ell_t$ for three-dimensional systems with index matched boundaries (neglecting internal reflections) [31], when $L \gg \ell_t$ the contribution of z_e to L_e is negligible ($L_e \simeq L$) and thus $z = d_w = 2$. However, for our homogeneous sample with $\ell_t = 40 \mu\text{m}$ and thicknesses in the range $230 \leq L \leq 450 \mu\text{m}$, we expect a difference between z and d_w . This is evident also from Fig. 2(b), where $z = d(\ln\tau_D)/d(\ln L)$ is reported as a function of the optical thickness L/ℓ_t . The exponent z obtained in the thickness range under consideration is in good agreement with the experimentally retrieved value ($z = 1.6 \pm 0.2$) and the limit $z \rightarrow d_w = 2$ is reached only for thicker samples.

Since there is currently no theory available to calculate the extrapolation length for Lévy glasses, we use the diffusive case as a starting point and assume that the relation $z_e = \frac{2}{3}\ell_t = \frac{2}{3}\langle\ell\rangle$ provides at least the right order of magnitude of the extrapolation length [32]. Both homogeneous samples and Lévy glasses were prepared to have the same mean step length [22], which simplifies the analysis. Power-law fits of the lifetime data using $\tau = cL_{\text{eff}}^{d_w}$ are shown in Fig. 2(c) and the results are summarized in Table I. The scaling exponent d_w obtained for the homogeneous sample is fully consistent with diffusive transport and those for the Lévy glasses are markedly smaller than 2.

C. Data collapse

It is interesting to visualize and analyze the collapse of the time-resolved transmission curves expected from the scaling hypothesis in Eq. (2) (with L_{eff} instead of L). Results are shown in Fig. 3. The time axis was

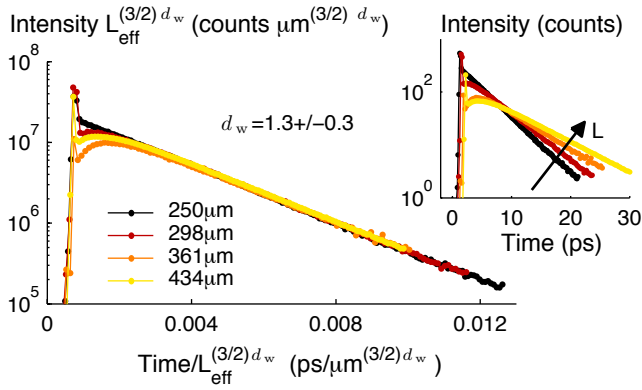


FIG. 3. (Color online) Collapse of the time-resolved transmission measured on Lévy glasses. An appropriate rescaling of the axes, according to Eq. (2) with the experimentally retrieved d_w and $\gamma = -\frac{3}{2}d_w$, yields a collapse of the time-resolved transmission curves obtained from samples with different thicknesses onto a single invariant profile. In the inset data are plotted by using regular axes and the dependence of the long-time decay on the growing thickness is marked by the arrow. The collapse obtained by rescaling the axes shows that the (anomalous) transport dynamics is described by a unique scaling exponent d_w .

rescaled as $t \rightarrow t/L_{\text{eff}}^{d_w}$. Regarding the transmission axis, we found that a very good collapse of the exponential tails for all systems investigated here was obtained using $T \rightarrow TL_{\text{eff}}^{3d_w/2}$, i.e. by taking $\gamma = -\frac{3}{2}d_w$ in Eq. (2). Quite remarkably, this is the value expected for annealed Lévy walks (See Appendix C).

The overall superposition of the transmission curves is excellent, showing that the measured scaling exponent d_w constitutes a unique parameter describing anomalous dynamics in these systems. The deviation at early times is also expected since the quasi-ballistic trajectories do not obey the scaling hypothesis that describes the spreading of the superdiffusive propagator. This is again typical of Lévy walk dynamics [33, 34].

IV. CONCLUDING REMARKS

We conclude by discussing some interesting points for future investigation. First, the standard approach to deal with the finiteness of open disordered systems, via the extrapolation length, should be revisited to take into account non-exponential step length distributions. For power-law distributions, this problem is directly related to the treatment of boundaries in the presence of spatial nonlocality [35]. Second, our scaling analysis has been performed on a restricted thickness range while it would be interesting to investigate, both experimentally and theoretically, the limit towards infinite system size [36, 37]. With respect to this important issue, there will be a difference between the case of fixed filling

fraction of heterogeneities, and that of maximal filling. A recent numerical study on two-dimensional (2D) systems [37] has shown that the fixed filling fraction case eventually leads to normal diffusion, while the maximal filled case leads to superdiffusion, provided that the system converges towards 100% voids surrounded by point scatterers. It is hence of fundamental importance to define properly how the limit to infinite system size is taken. Third, the scaling exponents retrieved experimentally here do not fully match with those expected from a “chord-length” model, i.e. $d_w = \beta - 1$ [18, 19]. Indeed, this simplified model neglects the possibility of crossing multiple voids in one step and of having correlations between successive steps due to quenched disorder, which are both expected to affect the dynamics [22, 36–39], and which deserve further attention.

In summary, we have presented a first experimental investigation of the walk dimension d_w for light waves in disordered photonic structures. The retrieval of d_w is possible via a scaling analysis of the lifetime, and allows one to distinguish clearly between regular and superdiffusive transport dynamics in Lévy glasses. These results show how the photonics of disorder can be used in the research on anomalous transport [7, 9], and that it can provide a new setting to investigate wave diffusion on fractal media [40, 41]. It will be interesting to investigate how the fractal dimension plays a role in interference effects, like weak and strong localization [42], where the dimensionality of the system can make a crucial difference between the occurrence of extended or localized states.

ACKNOWLEDGMENTS

We wish to acknowledge Raffaella Burioni, Alessandro Vezzani, Enrico Ubaldi, Sepideh Zakeri, Marco Grisi, and the entire *Optics of Complex Systems* group at LENS for fruitful discussions, Thomas Huisman and Lorenzo Pattelli for their help with sample preparation, and financial support from the European Research Council (FP7/2007-2013), ERC grant agreement n° [291349]. T.S. acknowledges funding from The Swedish Research Council (Grant 2010-887), K.V. from LABEX WIFI under references ANR-10-LABX-24 and ANR-10-IDEX-0001-02 PSL*.

Appendix A: Sample manufacturing

1. Lévy glasses

Lévy glasses (see Fig. 4) are obtained by first dispersing homogeneously the TiO₂ nanoparticles (Huntsman Tioxide R-XL, diameter 280 nm, refractive index 2.4) in a monomer host (acrylate optical glue Norlan 65, refractive index 1.52) and then by introducing Soda Lime glass microspheres (Duke Standards, refractive index 1.5) of

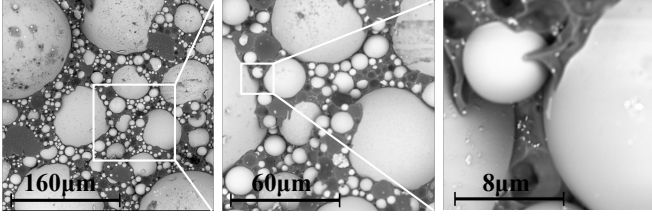


FIG. 4. Sequence of Scanning Electron Micrographs of the surface of a Lévy glass with increasing magnification that reveals the statistical self-similarity of the heterogeneity. The hosting polymer appears in dark gray while the glass spheres (typically with $5 \leq \phi \leq 400 \mu\text{m}$) in light gray. In the last close-up the TiO_2 nanoparticles are clearly distinguishable.

different diameters. The spheres filling fraction is 71% and the nanoparticles concentration is 1%. Due to the high refractive index contrast nanoparticles scatter light while glass spheres function only as spacers since they are index matched with the monomer. The diameters ϕ_i of the spheres categories are as follows: 5, 8, 10, 15, 20, 30, 40, 50, 70, 100, 120, 140, 170, 200, 230, 280, 330, and $400 \mu\text{m}$. The power-law probability density to find a sphere of diameter ϕ_i is obtained by distributing the number of spheres for each category as $N_i = C(\beta)\phi_i^{-(\beta+1)}$, where β can be arbitrary changed. The smaller β the higher the probability of finding large spheres. The constant $C(\beta)$ depends on the total number of spheres in the samples. Samples are manufactured in a slab geometry by squeezing the mixture between two microscope glass slides (index matched with the monomer) until the sample thickness matches the largest sphere diameter. Different thicknesses L are obtained by removing all the spheres categories with a diameter larger than L . The amount of monomer and of nanoparticles grows with L , but the spheres filling fraction and the nanoparticles concentration are kept fixed. For each spheres category the diameters are distributed around the mean value ϕ_i and since the thickness is determined by the few biggest values the measured L can deviate from the nominal ϕ_i by a 10%. The reported L do not contain the thickness of the slides. In the final stage samples are exposed to UV radiation for polymerization to “freeze” the components position.

2. Homogeneous reference samples

In the homogeneous reference samples microspheres are substituted with an equivalent volume of monomer, which leaves the final mixture fluid. The slab geometry is obtained by first preparing a hosting cell of the desired L with the same microscope slides used for the Lévy glasses. The scattering monomer is inserted in the cell by means of infiltration. In the final stage samples are exposed to UV radiation for polymerization.

Appendix B: Experimental Setup

1. Optical gating

The setup (see Fig. 5) is based on an optical gating technique [23–25] and involves the use of two ultrashort pulses ($\approx 130 \text{ fs}$) of different frequencies ω_1 and ω_2 , whose wavelengths are respectively $\lambda_1=810 \text{ nm}$ and $\lambda_2=1540 \text{ nm}$. Pulses at ω_1 are generated at a repetition rate of 82 MHz by a Ti:Sapphire mode-locked laser (*Tsunami*, Spectra Physics) pumped by a continuous-wave laser (*Millenia*, Spectra Physics). Pulses at ω_2 are obtained by converting the pulse train at ω_1 through an Optical Parametric Oscillator (*Opal*, Spectra Physics). The probe pulse at ω_1 is incident onto the sample, interacts with its structure, and emerges with a stretched temporal profile $I_{\omega_1}(t)$. The gate pulse at ω_2 travels undisturbed with its Gaussian temporal profile $I_{\omega_2}(t)$ on an independent line. The two optical signals are overlapped, in space and in time, into an optical non-linear crystal *beta*-BBO (*beta*-barium borate) which generates the sum-frequency $I_{\omega_1+\omega_2}(t_d) \propto \int_0^\infty I_{\omega_1}(t)I_{\omega_2}(t-t_d)dt$, where t_d is their relative time delay. Being the evolution of $I_{\omega_1}(t)$ much slower than that of $I_{\omega_2}(t)$, the latter can be approximated by a δ -function so that the previous convolution becomes $I_{\omega_1+\omega_2}(t_d) \propto I_{\omega_2}I_{\omega_1}(t_d)$. By measuring the stationary signal $I_{\omega_1+\omega_2}(t_d)$ for different delays t_d we retrieve the temporal profile $I_{\omega_1}(t)$ of the transmitted intensity.

2. Setup configuration

The delay t_d is changed by varying the optical path of the probe pulse through a motorized translation stage. The sum-frequency is detected by a photomultiplier tube. Background noise suppression is obtained by chopping the beam (20 Hz) and by using a Gated Integrator Pho-

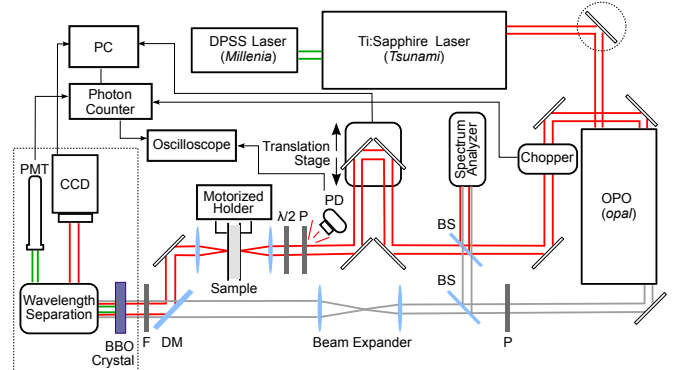


FIG. 5. (Color online) Schematic of the experimental setup based on an optical gating technique: BS, beam splitter; P, polarizer; $\lambda/2$, half wave plate; DM, dichroic mirror; F, filter; PD, photodiode; PMT, photo multiplier tube. Dot contours indicate covering boxes.

ton Counter. A synchronization of the acquiring temporal window is obtained by monitoring both the optical and the electronic trigger signals through an oscilloscope. The injection and collection lenses are selected so as to image the whole transmitted profile on the BBO.

3. Non linear conversion

The phase-matching conditions on the BBO crystal are optimized for parallel collimated beams, implying that among the transmitted multiply scattered k-vectors only the forward directed ones are efficiently converted. The distribution of transmitted k-vectors is fully randomized (Lambertian distribution) after few scattering events and it is time-independent. It follows that the time evolution of the measured intensity gives a correct representation of the time evolution of the total transmission since they are proportional at every instant through a time-independent constant. The correct functioning of the setup has been carefully tested on homogeneously disordered samples in a previous publication [24].

Appendix C: Collapse on the intensity axis

It is theoretically predicted that the steady-state total transmission $T(L) = \int_0^\infty T(t, L)dt$ for annealed Lévy walks with fractal dimension $d_w < 2$ through a slab of thickness L scales as

$$T(L) \sim L^{-d_w/2},$$

which is a generalized Ohm's law valid in the limit of very large L , where finite-size effects can be neglected [17, 43].

In this case the value of the exponent γ in Eq. (2) can be derived by rewriting Eq. (2) as [30]

$$T(t, L) = L^\gamma \tilde{T}(t/L^{d_w}),$$

and by imposing

$$T(L) = \int_0^\infty T(t, L)dt = L^\gamma \int_0^\infty \tilde{T}\left(\frac{t}{L^{d_w}}\right) \sim L^{-d_w/2}.$$

By changing integration variable as $t \rightarrow t/L^{d_w}$ the previous similarity implies $\gamma = -\frac{3}{2}d_w$.

We have applied this result to our case of finite-size samples by considering their effective thickness L_{eff} instead of the physical thickness L .

-
- [1] F. Reif, *Fundamentals of statistical and thermal physics* (Waveland Press, 2009).
 - [2] O. Bénichou, C. Loverdo, M. Moreau, and R. Voituriez, *Reviews of Modern Physics* **83**, 81 (2011).
 - [3] D. Brockmann, L. Hufnagel, and T. Geisel, *Nature* **439**, 462 (2006).
 - [4] E. Barkai, Y. Garini, and R. Metzler, *Physics Today* **65**, 29 (2012).
 - [5] A. Ishimaru, *Wave Propagation and Scattering in Random Media*, IEEE Press Series on Electromagnetic Wave Theory (IEEE Press, 1999).
 - [6] A. Marshak and A. A. B. Davis, *3D radiative transfer in cloudy atmospheres* (Springer, 2005).
 - [7] D. Ben-Avraham and S. Havlin, *Diffusion and Reactions in Fractals and Disordered Systems* (Cambridge Univ. Press, 2000).
 - [8] M. E. Cates, *Journal de Physique* **46**, 1059 (1985).
 - [9] R. Klages, G. Radons, and I. M. Sokolov, *Anomalous Transport: Foundations and Applications* (Wiley-VCH, 2008).
 - [10] S. Condamin, O. Benichou, V. Tejedor, R. Voituriez, and J. Klafter, *Nature* **450**, 77 (2007).
 - [11] Y. Li, G. Farrher, and R. Kimmich, *Physical Review E* **74**, 066309 (2006).
 - [12] B. Berkowitz, H. Scher, and S. E. Silliman, *Water Resources Research* **36**, 149 (2000).
 - [13] M. Palombo, A. Gabrielli, S. De Santis, C. Cametti, G. Ruocco, and S. Capuani, *The Journal of chemical physics* **135**, 034504 (2011).
 - [14] I. M. Tolić-Norrelykke, E.-L. Munteanu, G. Thon, L. Oddershede, and K. Berg-Sørensen, *Physical Review Letters* **93**, 078102 (2004).
 - [15] I. Golding and E. C. Cox, *Physical Review Letters* **96**, 098102 (2006).
 - [16] J. Szymanski and M. Weiss, *Physical Review Letters* **103**, 038102 (2009).
 - [17] A. Davis and A. Marshak, in *Fractal Frontiers*, edited by M. M. Novak and T. G. Dewey (World Scientific, Singapore, 1997) pp. 63–72.
 - [18] P. Barthelemy, J. Bertolotti, and D. S. Wiersma, *Nature* **453**, 495 (2008).
 - [19] J. Bertolotti, K. Vynck, L. Pattelli, P. Barthelemy, S. Lepri, and D. S. Wiersma, *Advanced Functional Materials* **20**, 965 (2010).
 - [20] N. Mercadier, W. Guerin, M. Chevrollier, and R. Kaiser, *Nature physics* **5**, 602 (2009).
 - [21] Q. Baudouin, R. Pierrat, A. Eloy, E. Nunes-Pereira, P.-A. Cuniasse, N. Mercadier, and R. Kaiser, arXiv:1402.6200 (2014).
 - [22] T. Svensson, K. Vynck, M. Grisi, R. Savo, M. Burreli, and D. S. Wiersma, *Physical Review E* **87**, 022120 (2013).
 - [23] J. Shah, *Quantum Electronics, IEEE Journal of* **24**, 276 (1988).
 - [24] T. Svensson, R. Savo, E. Alerstam, K. Vynck, M. Burreli, and D. S. Wiersma, *Optics letters* **38**, 437 (2013).
 - [25] D. S. Wiersma, A. Muzzi, M. Colocci, and R. Righini, *Physical Review Letters* **83**, 4321 (1999).
 - [26] J. Bertolotti, K. Vynck, and D. S. Wiersma, *Physical Review Letters* **105**, 163902 (2010).
 - [27] M. Burreli, V. Radhalakshmi, R. Savo, J. Bertolotti, K. Vynck, and D. S. Wiersma, *Physical Review Letters* **108**, 110604 (2012).

- [28] E. Akkermans and G. Montambaux, *Mesoscopic physics of electrons and photons* (Cambridge University Press, 2007).
- [29] The early-time transmission cannot be fitted due to a transient failure of diffusion theory in thin slabs ($L/\ell_t < 10$) [44]. Hence the fit is taken over a range that starts around the maximum and covers the entire tail. This corresponds to the range over which the grey line is drawn.
- [30] P. Buonsante, R. Burioni, and A. Vezzani, *Physical Review E* **84**, 021105 (2011).
- [31] M. C. W. van Rossum and T. M. Nieuwenhuizen, *Reviews of Modern Physics* **71**, 313 (1999).
- [32] The precise determination of the extrapolation length is complicated even in regular diffusive samples and is influenced e.g. by internal reflection. Recent elaborate numerical studies, which will be published elsewhere, indicate that indeed z_e remains of the order of ℓ .
- [33] P. Drysdale and P. Robinson, *Physical Review E* **58**, 5382 (1998).
- [34] G. Zumofen and J. Klafter, *Physical Review E* **47**, 851 (1993).
- [35] A. Zoia, A. Rosso, and M. Kardar, *Physical Review E* **76**, 021116 (2007).
- [36] C. W. Groth, A. R. Akhmerov, and C. W. J. Beenakker, *Physical Review E* **85**, 021138 (2012).
- [37] R. Burioni, E. Ubaldi, and A. Vezzani, *Physical Review E* **89**, 022135 (2014).
- [38] P. Barthelemy, J. Bertolotti, K. Vynck, S. Lepri, and D. S. Wiersma, *Physical Review E* **82**, 011101 (2010).
- [39] T. Svensson, K. Vynck, E. Adolfsson, A. Farina, A. Pifferi, and D. S. Wiersma, *Physical Review E* **89**, 022141 (2014).
- [40] E. Akkermans, G. V. Dunne, and A. Teplyaev, *Physical Review Letters* **105**, 230407 (2010).
- [41] A. A. Fernández-Marín, J. A. Méndez-Bermúdez, and V. A. Gopar, *Physical Review A* **85**, 035803 (2012).
- [42] P. Sheng, *Introduction to Wave Scattering, Localization and Mesoscopic Phenomena*, Springer Series in Material Science (Springer-Verlag, Berlin, Heidelberg, 2006).
- [43] S. V. Buldyrev, S. Havlin, A. Y. Kazakov, M. G. E. da Luz, E. P. Raposo, H. E. Stanley, and G. M. Viswanathan, *Physical Review E* **64**, 041108 (2001).
- [44] R. Elaloufi, R. Carminati, and J.-J. Greffet, *J. Opt. Soc. Am. A* **21**, 1430 (2004).